

Symmetry Analysis of Second Harmonic Generation at Surfaces of Antiferromagnets

M. Trzeciecki^{1,3}, A. Dähn², and W. Hübner¹

¹*Max-Planck-Institut für Mikrostrukturphysik, Weinberg 2, D-06120 Halle, Germany*

²*Institute for Theoretical Physics, Freie Universität Berlin, Arnimallee 14, D-14195 Berlin, Germany*

³*Institute of Physics, Warsaw University of Technology, Koszykowa 75, 00-662 Warsaw, Poland*
(July 8, 2021)

Using group theory we classify the nonlinear magneto-optical response at low-index surfaces of fcc antiferromagnets, such as NiO. Structures consisting of one atomic layer are discussed in detail. We find that optical second harmonic generation is sensitive to surface antiferromagnetism in many cases. We discuss the influence of a second type of magnetic atoms, and also of a possible oxygen sublattice distortion on the output signal. Finally, our symmetry analysis yields the possibility of antiferromagnetic surface domain imaging even in the presence of magnetic unit-cell doubling.

78.20.Ls, 75.30.Pd, 75.50.Ee, 42.65.-k

I. INTRODUCTION

Optical Second Harmonic Generation (SHG) has been proven to be a very useful technique for the investigation of ferromagnetism at surfaces. The obvious question is if this technique can also yield some new information in the case of more general spin configurations, such as antiferromagnetic (AF) ordering. An experimental answer to this question has been provided by Fiebig *et al.* [1], who obtained a pronounced optical contrast from AF 180° domains of rhombohedral bulk Cr₂O₃. The authors attributed this contrast to the interference of magnetic and electric dipole contributions, the latter being present only below the Néel temperature. Since it is known that, in *cubic* materials, within the electric dipole approximation, optical SHG originates only from surfaces, interfaces, or thin films, an important question is if SHG is also sensitive to antiferromagnetism at surfaces of cubic antiferromagnets. In this paper, we will show that the surface of a cubic material can lower the symmetry of an AF fcc crystal (two-sublattice antiferromagnet) in a way similar to the trigonal distortion in a four sublattice antiferromagnet Cr₂O₃. Besides, even the imaging of AF *domains* is possible also for many cubic materials that exhibit unit-cell doubling.

The first theoretical explanation of *linear* magneto-optic effects in ferromagnets has been given by Argyres [2] in the 50s. He used linear response theory for current-current correlation functions. His microscopic explanation was already based on the combination of spin-orbit and exchange coupling. Experimental techniques for the detection of AF domain *walls* using linear optics in some special geometries were elaborated a few years later [3]. The *interior* of the domains has been visualized in piezoelectric AF crystals using a linear magneto-optical effect [4]. However, linear optical experiments suffer from mixing the desired signal with a contribution from other lin-

ear effects, such as birefringence or dichroism. A review of linear optical experimental methods for the investigation of AF domains is given by Dillon [5].

The observation of domain structure in antiferromagnets is more complicated than in ferromagnetic materials since the reduction of the spatial symmetry is, unlike for ferromagnets, not linked to an imbalance in the occupation of majority and minority spin states. On the basis of group theoretical considerations, Brown *et al.* [6] proposed the use of linear optical effects, namely gyrotropic birefringence, for the observation of AF domains related to each other by the space-inversion operation. A theoretical review of effects found by a group-theoretical approach is presented by Eremenko and Kharchenko [7]. They performed a comprehensive study of linear optical effects for various AF materials. Another effect proposed recently by Dzyaloshinskii *et al.* [8] gives a possibility to detect antiferromagnetism taking advantage from optical path differences from antiferromagnetically coupled but intrinsically ferromagnetic planes.

Nonlinear optics exhibits an additional degree of freedom, since its elementary process involves three photons instead of two in linear optics. For that reason, some authors, e.g. Fröhlich [9] suggested the application of nonlinear optics even for k-selective spectroscopy, since multi-photon phenomena allow for the “scanning” of a small part of the Brillouin zone, at least for semiconductors. Recently, non-linear optics has attracted more and more attention for the investigation of magnetism due to its enhanced sensitivity to twodimensional *ferromagnetism* [10]. The magnetic effects are usually much stronger than in linear optics (rotations up to 90°, pronounced spin polarized quantum well state oscillations [11,12], magnetic contrasts close to 100%) [13,14]. An example of ferromagnetic effects measurable only by SHG deals with the existence of surface magnetism in very thin films of Fe/Cu(001) and is given in Ref. [15]. Nonlinear

optical effects were invoked to explain the behavior of lasers in magnetic fields [16], to investigate high temperature superconductors [17,18], and to study structures composed from alternately ferro- and antiferromagnetically ordered thin films [19]. One of the first theoretical investigations of the possibility to apply nonlinear optics to *antiferromagnetism* was performed by Kielich and Zawodny [20]. However, the first experiments concerning the detection of the AF domains in materials such as Cr_2O_3 were carried out only recently [21,22]. Already in the 70s, it has been proposed [23] that experimental studies of dc magnetic and electric field-induced SHG could become an effective method of determining the crystal structure of solids, the symmetry of which cannot be investigated by other methods. Extending this idea towards surface crystallography provides us with a new technique for determining the spin configuration in a given surface structure. In turn, it permits to use a known magnetic configuration for the determination of the surface structure. All the mentioned effects are more difficult or even impossible to obtain in linear optics, and moreover other linear methods like neutron scattering have difficulties to probe AF spin configurations.

The nonlinear magneto-optical susceptibility tensor $\chi_{el}^{(2\omega)}$ (the source for SHG within the electric dipole approximation) has predominantly been investigated from the symmetry point of view. A classification following this approach, with tensors of a rank up to six, has been performed by Lyubchanskii *et al.* [24–26,13,27]. In Ref. [13] the authors include the magnetization-gradient terms and apply the group-theoretical classification to higher-rank susceptibility tensors. This approach then allows them to study the thickness and the character (Bloch vs. Néel type) of domain walls. An attempt by Muthukumar *et al.* [28] to calculate the $\chi_{el}^{(2\omega)}$ tensor elements for the antiferromagnetic Cr_2O_3 both from group theory as well as *from the microscopic point of view* is rather unique. They implemented a $(\text{CrO}_6)_2$ cluster, thus taking into account only half of the spins present in the elementary magnetic cell. In this approximation they explained the SHG from Cr_2O_3 as observed by Fiebig *et al.* [1] and they were able to give a quantitative estimate for that. Tanabe *et al.* [29], however, pointed out that the occurrence of purely real or imaginary values of the tensor elements plays a decisive role for the existence of SHG from this substance. They found that for a $(\text{CrO}_6)_2$ cluster SHG can take place only in the case where the tensor elements are imaginary, and thus should vanish in Muthukumar’s approximation. They proposed to take into account the full unit cell with four inequivalent Cr ions including their “twisting” interaction with the environment. However Tanabe *et al.* neglected the dissipation in the process of SHG [30], which is a rather crude approximation. In general, taking into account the dissipation makes the $\chi_{el}^{(2\omega)}$ tensor elements complex and

invalidates their separation in purely real and imaginary ones [31].

Lifting the inversion symmetry of a crystal is the source for SHG. Lyubchanskii *et al.* [24,26] suggested crystal lattice deformations and displacements as possible reasons for SHG from YIG films. In the case of Cr_2O_3 and $\text{YBa}_2\text{Cu}_3\text{O}_{6+\delta}$, described by Lyubchanskii *et al.* [25,26], AF ordering lowers the symmetry of an otherwise centrosymmetric crystal. In this paper, however, we rely on the idea that, rather than lowering the crystal symmetry in the bulk, SHG may also result from the breaking of inversion symmetry at the surface of a bulk inversion-symmetric system.

Magnetically active oxide layers are of importance for the construction of TMR (tunneling magnetoresistance) devices, where a trilayer structure is commonly used. The central layer of TMR devices consists of an oxide sandwiched between a soft and a hard magnetic layer (these two layers are often composed from the same material but of different thicknesses). For these technological applications it is necessary to develop a technique to study buried oxide interfaces. Such a technique can be SHG. One of the most promising materials for the mentioned devices is NiO. However, to the best of our knowledge, the understanding of its detailed spin structure is scarce - even the spin orientation on the ferromagnetically ordered (111) surfaces is not known. The technique presented here can shed some light on that issue.

Our paper is organized as follows: in Sec. II we present our methods for obtaining sets of nonvanishing $\chi_{el}^{(2\omega)}$ tensor elements. In Sec. III we present the results of our analysis, first for the nondistorted surface of a simple fcc structure (subsection III.A), then for the distorted one (III.B). Subsequently, we discuss the influence of a second kind of magnetic atoms (III.C) and of oxygen sublattice distortion (III.D). The issue of domain imaging is addressed in subsection III.E. Possible experimental geometries allowing for the detection of the mentioned structures and effects are discussed in Sec. IV. The conclusions are presented in Sec. V.

II. THEORY

Based on group theory, Dähn *et al.* [32] proposed a new nonlinear magneto-optic Kerr effect (NOLIMOKE) at the surface of cubic antiferromagnets. They also gave an example of an antiferromagnetic structure (NiO) and an optical configuration, where this new effect could be observed. Here, we perform a complete group-theory based analysis of collinear AF fcc low-index crystal surfaces. Surfaces of other crystal structures are as well described by our theory provided they are similar to fcc crystal surfaces, i.e. squares or hexagons. The results can be used to detect the magnetic order of a specific surface under investigation and allow for the determination of the surface

spin configuration in some important cases. However, in order to calculate the SHG yield quantitatively, it is necessary to go beyond the present study and use electronic calculations of the nonlinear susceptibility. Group theory can give a unified picture of different experimental observations and predict new effects [33], while the microscopic origins of the observed phenomena may remain unclear. In order to be clear with respect to the essential notion of time reversal we would like to emphasize the point of view taken in this paper in the beginning. Here, we do not divide $\chi_{el}^{(2\omega)}$ into even and odd parts in the magnetic order parameter. Instead, the behavior of $\chi_{el}^{(2\omega)}$ with respect to the magnetic order parameter (which for ferromagnetic materials corresponds to the dependence of $\chi_{el}^{(2\omega)}$ on magnetization) is fully taken into account by the considerations of the magnetic point group. At no stage of our consideration we invoke the notion of time reversal, consequently we do not apply the characterization of the susceptibility $\chi^{(2\omega)}$ as c-tensor (changing its sign in the time-reversal operation) or i-tensor (invariant under the time-reversal operation) [31].

Before we start our group theoretical classification of the nonlinear optical susceptibilities of AF surfaces we would like to emphasize the following four important points:

(i) We are not interested in effects resulting from the *optical path difference* from adjacent crystal planes which are ferromagnetically ordered but only antiferromagnetically coupled to each other. We do not consider this as an intrinsic AF effect.

(ii) Cubic crystals that we are interested in reveal a center of inversion in the para-, ferro-, and all antiferromagnetic phases. Thus, within the electric dipole approximation, the SHG signal from the bulk vanishes.

(iii) While in principle linear optical methods can be sensitive to the presence of a spin structure, in practice they are not useful because, within the group theoretical approach, they cannot distinguish the AF phase from either paramagnetic or ferromagnetic, nor can they distinguish different AF configurations from each other. They have to resort to methods like lineshape analysis, where no strong statements characteristic for symmetry analysis can be made.

(iv) Although the tensor elements for all the magnetic point groups are known and tabulated in the literature (e.g. [34]), the connection between the different spin configurations described by us and the mentioned symmetry groups has not been made, except for some easy cases [32]. Thus, for SHG from antiferromagnetic surfaces there has been up to now no connection between the group theoretical classification and the real situations found in experiments.

The following part of the text should explain the fundamentals of applying NOLIMOKE observations to investigate antiferromagnetism of surfaces.

Now we turn to SHG, the source of which is the nonlinear electrical polarization $P_{el}^{(2\omega)}$ given by:

$$P_{el}^{(2\omega)} = \epsilon_0 \chi_{el}^{(2\omega)} : E^{(\omega)} E^{(\omega)}. \quad (1)$$

Here, $E^{(\omega)}$ is the electric field of the incident light, while $\chi_{el}^{(2\omega)}$ denotes the nonlinear susceptibility within the electric dipole approximation, and ϵ_0 is the vacuum permittivity. The intensity of the outgoing SHG light is [35]:

$$I^{(2\omega)} \sim (I_0)^2 \left[F(\Theta, \Phi, 2\omega) \times \begin{pmatrix} \chi_{xxx} & \chi_{xyy} & \chi_{xzz} & \chi_{xyz} & \chi_{xzx} & \chi_{xxy} \\ \chi_{yxx} & \chi_{yyy} & \chi_{yzz} & \chi_{yyz} & \chi_{yzy} & \chi_{yyx} \\ \chi_{zxx} & \chi_{zyy} & \chi_{zzz} & \chi_{zyz} & \chi_{zzx} & \chi_{zxy} \end{pmatrix} \times f(\vartheta, \varphi, \omega) \right]^2 \quad (2)$$

where I_0 is the intensity of the incident light, $F()$ ($f()$) describe Fresnel and geometrical factors for the incident (reflected) light, ϑ and Θ angles of incidence and reflection, respectively ($\vartheta = \Theta$), and Φ (φ) is output (input) polarization angle. According to Neumann's principle, "any type of symmetry which is exhibited by the crystal is possessed by every physical property of the crystal" [34]. To examine these physical properties, we determine the magnetic point group of the crystal lattice, thus determine its symmetries. The same symmetries must leave the investigated property tensor (in our case the nonlinear electric susceptibility $\chi_{el}^{(2\omega)}$) invariant. This fact is mathematically expressed by the following condition:

$$\chi_{el, i'j'k'}^{(2\omega)} = l_{i'i} l_{j'j} l_{k'k} \chi_{el, ijk}^{(2\omega)}, \quad i, j, k, i', j', k' = x, y, z. \quad (3)$$

Here, $l_{n,n'}$ ($n = i, j, k, n' = i', j', k'$) is a representation of an element of the magnetic point group describing the crystal. For symmetry operations including the time reversal there should be an additional "±" sign in Eq.(3), but we do not use it here since we exclude the time reversal from our consideration. In particular, from Eq.(3) it follows immediately that polar tensors of odd rank (such as $\chi_{el}^{(2\omega)}$) vanish in inversion symmetric structures. This explains why SHG is possible only at surfaces and interfaces, where this symmetry is broken. For a given spin configuration we apply Eq. (3) for every symmetry operation exhibited by the system. Thus, each of these symmetries gives rise to a set of 27 equations with 27 unknown elements of the tensor $\chi_{el}^{(2\omega)}$. This set can be reduced to 18 equations, since

$$\chi_{el, ijk}^{(2\omega)} = \chi_{el, ikj}^{(2\omega)}, \quad (4)$$

which expresses the equivalence of the incident photons of frequency ω , see also the reduced notation in Eq. (2). The analytic solution of even this reduced set of equations seems cumbersome, but the set can be split into

several decoupled subsets. For example, an obvious subset in every case is the equation $\chi_{zzz} = \chi_{zzz}$, this tensor element occurs nowhere else. The rank of other subsets is, for our cases, never higher than six. In this manner, one may obtain a set of forbidden elements of the susceptibility tensor as well as relations between existing ones.

III. RESULTS

First, we will define the notions of “phase”, “case”, and “configuration”, used henceforth to classify our results. “Phase” describes the magnetic phase of the material, i.e. paramagnetic, ferromagnetic, or AF. Secondly, the word “configuration” is reserved for the description of the magnetic ordering of the surface. It describes various possibilities of the spin ordering, which are different in the sense of topology. We describe up to 18 AF configurations, denoted by little letters a) to r), as well as several ferromagnetic configurations, denoted as “ferro1”, “ferro2”, etc. The number of possible configurations varies depending on surface orientation. Thirdly, we describe different “cases”, i.e. additional structural features superimposed on the symmetry analysis. “Case A” does not have such additional features. In “case B” we address distortions of the lattice. “Case C” deals with two kinds of magnetic atoms in an undistorted lattice. In “case D” we take into account a distorted sublattice of nonmagnetic atoms, keeping the magnetic sublattice undistorted. All the analysis concerns collinear antiferromagnets, with one easy axis.

The tables show the SHG response types for each configuration. The various response types are encoded by a “key”, which is then decoded in Tab. I. This table presents the symmetries, domain operations, and non-vanishing tensor elements for each response type. This is done in order to shorten the overall length of tables, because a given response type can appear in several different cases.

Several spin structures depicted in Fig. 1 and Fig. 5 are distinct configurations only in case B, and they are addressed in the tables that concern only this case. For the rest of the cases they are domains of other, fully described configurations, thus they are left out in these cases. The philosophy of the paper is that, to save some space, we show the spin structure in one figure for each surface (Fig. 1, 4, and 5) for all the four cases (A-D), and depict the effects taken into account in the cases B-D only for the paramagnetic phase (Fig 6, 7, and 8). Table I also contains the information on the parity of the nonvanishing tensor elements: the odd ones are printed in boldface. In some situations an even tensor element (shown in lightface) is equal to an odd element (shown in boldface), this means that this pair of tensor elements is equal in the domain which is depicted on the corresponding figure, but they are of opposite sign in the other

domain. This happens in the structures where two pairs of domains are possible (two distinct entries in Table I). The tensor elements that change their parity in the domain operation which is the inverse of the displayed one are shown in italic font. For example, the entry j) of Table I shows a tensor element *xxx*, which is even under the operation 4_z , this means that this tensor element is odd under -4_z . This strange at the first sight behavior of tensor elements is caused by the fact that under these operations, tensor elements are not mapped on themselves. In our example, after applying 4_z the tensor element *xxx* becomes *yyy*, without changing its sign. If we now apply -4_z , *yyy* (which is now even) becomes *xxx*, again without changing the sign.

The parity of the elements has been checked in the operations 2_z , 4_z , and in the operation connecting mirror-domains to each other (for the definition of the mirror-domain structure see subsection E). The domain operation(s) on which the parity depends is (are), if applicable, also displayed in this Table. If two or more domain operations have the same effect, we display all of them together. To make the Table I shorter and more easily readable some domain operations (and the corresponding parity information for the tensor elements) are not displayed, namely those that can be created by a superposition of the displayed domain operations. We also do not address the parity of tensor elements in the 6_z nor 3_z operations for (111) surfaces nor any other operation that “splits” tensor elements, although these operations also lead to a domain structure [36]. As will be discussed later (subsection E) it is possible to define a parity of the tensor elements for the 3_z and 6_z operations, however the tensor elements then undergo more complicated changes. The situations where the parity of the tensor elements is too complicated to be displayed in the Table are indicated by a hyphen in the column “domain operation”. For some configurations, none of the operations leads to a domain structure - in those configurations we display the information “one domain”. The reader is referred to the Appendix for the particularities of the parity check.

As far as the first layer is concerned, we address all the spin configurations of the low index surfaces of fcc antiferromagnets, with magnetic order vector lying in plane or perpendicular to it and antiferromagnetic coupling between nearest neighbors. For the (001) surfaces we also discuss the configurations, where the antiferromagnetic coupling exists between the second-nearest neighbors (configurations a), b), c), f), and o), along with d), g), and h) for case B.). We do not consider the coupling to the third and further neighbors. This would not give rise to configurations of different symmetries in two dimensions. It may at most replace spins by grains (blocks) of spins in the configurations described by us.

Throughout this paper we take into account the spin structure only of the first (uppermost) atomic layer. This is sufficient to study all the symmetries of (001) and

(110) surfaces both in the paramagnetic and ferromagnetic phases. For the (111) surface it is necessary to recognize the atomic positions (but not the spins) in the second layer for the same purpose. For the sake of completeness we also present a study of (111) surfaces without this extension. However, in the antiferromagnetic phase, the spin structure of the second and deeper layers plays a role in determining the symmetry of the surface. This is presented in this paper using the (001) surface as an example. For the (110) and (111) surfaces it will be published elsewhere [37]. These structures can serve as simple models for deriving predictions for more complicated cases, while the full consideration of the second layer would not bring any new interesting results. Taking into account the spin structure of the second layer (deeper layers do not bring up anything new to the analysis) results in creating several (up to two for the (001) surface and three for the (111) surface) configurations out of each one addressed here by us. The symmetry of these configurations may remain the same or be lowered (sometimes even below the symmetry of the ferromagnetic phase) with respect to the “two-dimensional” configurations they are generated from. Consequently the distinction of the configurations from each other may be limited, but the possibility to detect the magnetic phase is not severely affected. Also our remarks on domain imaging remain valid. However the number of domains is increased, thus the possibility to identify each of them might be hampered.

Consequently, one can state that the symmetry of an AF surface depends on two atomic layers. They are also necessary (and sufficient) to define AF bulk domains. As will be presented in our results, SHG can probe both these layers on AF surfaces.

A. Equivalent atoms

The predicted new nonlinear magneto-optical effects result from the fact that the magnetic point groups of antiferromagnetic configurations are different from those describing paramagnetic or ferromagnetic phases of the same surface. Since, depending on the magnetic phase, different tensor elements vanish, it is possible to detect antiferromagnetism optically by varying the polarization of the incoming light.

The current subsection discusses nonvanishing elements of the nonlinear susceptibility tensor for an fcc crystal consisting of only one kind of magnetic atoms. The influence of nonmagnetic atoms in the material will be discussed later. The configurations considered here are “ferro1”, “ferro2”, “ferro4”, a), b), c), e), f), i), k), m), o), p), and r) for the (001) surface (see Fig. 1), “ferro1”, ferro3”, “ferro5”, a), c), f), i), and k) for the (111) surface (see Fig. 5), and all configurations depicted

in Fig. 4 for the (110) surface. Other depicted spin structures form domains of these configurations and are not referred to in this subsection nor in the tables concerning the current subsection [38].

All possible configurations (confs.) of a fcc (001) surface are shown in Fig. 1, which displays the conventional rather than magnetic unit cells. However, these are sufficient to fix the spin configuration of the whole surface imposing of the following “convention”: the fcc surface is constructed from the depicted plaquette in the way that neighboring spins along the x and y directions point the same way (alternate) if they are parallel (antiparallel) on the plaquette in these two directions. The spins in rows and columns where only one spin is presented are continued in the same way as the corner spins. For instance in the configuration a) of the (001) surface, both the right-hand side and left-hand side neighbors of the “central” spin will point upwards, while the spin direction will be alternated along the x axis. This convention will be maintained henceforth (for a (111) surface one has to alter or keep the spins along three axes, instead of two). The smallest set that gives a complete idea about the spin structure is presented in Fig. 2 [39]; this “magnetic primitive cell” does not give a clear picture of the crystal symmetries, however. The whole crystal lattice can be reproduced by translations of this cell, without performing other operations such as reflections or rotations.

The SHG response types for the (001) monolayer are given in Table II, for the paramagnetic, ferromagnetic, and all AF phases. We can observe several sets of allowed tensor elements. The Conf. r) will produce the same signal as the paramagnetic phase. The Conf. “ferro1” reveals a completely different, distinguishable set of tensor elements. In addition, the conf. “ferro2” produces another set of tensor elements, different from any other configuration. It is equivalent to the conf. “ferro1” rotated by 45° . In the confs. a), b), e), and o) we find the same tensor elements as for the paramagnetic phase. However, due to the lower symmetry, their values are no longer related to each other. Confs. c) and f) bring new tensor elements, thus allowing for the distinction of these confs. from the previous ones. Confs. i), k), m), p) reveal the same tensor elements as c) and f) but some of these elements are related. Thus one may possibly distinguish these two sets of configurations. Conf. “ferro4” presents a completely different, distinguishable set of the nonvanishing tensor elements. Consequently, in six configurations (i.e. c), f), i), k), m), and p)) some susceptibility tensor elements appear only in the AF phase, allowing for the detection of this phase by varying the incident light polarization, as will be outlined in Sec. IV. In addition, all other antiferromagnetic configurations but r) reveal the breakdown of some of the relations between the different tensor elements, compared to the paramagnetic phase, and thus can be detected as well. Gener-

ally, all the phases can be distinguished from each other. There exists as well a possibility to distinguish different AF configurations provided the corresponding tensor elements can be singled out by the proper choice of the experimental geometry.

For the sake of completeness, we now present a short study of the (001) surface where the spin structure of the two topmost atomic layers is taken into account. The paramagnetic phase and all the ferromagnetic configurations remain unchanged with respect to the results of the previous paragraph (for the (001) monolayer). However, most of the AF configurations previously addressed break up into two different configurations (sometimes even with a different symmetry). These configurations are constructed from the ones of the previous paragraph by assuming that the structure of the second atomic layer is identical with that of the topmost one but shifted along the positive x axis (indicated by x after the name of the original configuration) or positive y axis (indicated by y after the name of the “parent” configuration) in a proper way to form a fcc structure; if only one configuration can be produced in this way we use the name of the original one. This construction is depicted in Fig. 3, along with the corresponding conventional unit cells for the two topmost layers of the AF fcc (001) surface. The resulting SHG response types are presented in Table III. In general, seven types of response are possible. Firstly, the paramagnetic phase reveals a characteristic set of tensor elements. Thus it can be unambiguously distinguished from any other magnetic phase. Secondly, confs. “ferro1”, (ax) , (ox) , (bx) , (by) , (ex) , and (ey) bring some additional tensor elements into play. The symmetry of confs. (ax) and (ox) is slightly different from the one of the rest of this group, since the mirror plane is rotated by 90° around the z axis. A different set of tensor elements is brought up by confs. “ferro2”, (i) , (m) , and (p) . The difference between the response yielded by conf. (i) and the other confs. in this group, due to a slightly different symmetry, can be compensated by rotating the sample by 90° around the z axis. Another, characteristic set of tensor elements is presented by conf. “ferro4” alone. The fifth type of SHG response is given by confs. (ay) , (oy) , and (r) . Tensor elements, that do not vanish in these configurations, are the same as for the paramagnetic phase but some relations between them are broken due to a lower symmetry in the AF phase. Confs. (cx) , (fx) , and (fy) yield all tensor elements in an unrelated way. The last, characteristic type of response is presented by conf. (k) alone. Consequently, the detection possibilities of an antiferromagnetic bilayer are slightly worse than those for a monolayer. Especially, a difficulty in distinguishing the ferromagnetic phase from the antiferromagnetic one may arise for some configurations where then the combination of SHG with linear magneto-optics is definitely required. There exists a possibility to distinguish AF configurations from each other, similarly to the previ-

ous situation. In most configurations, the difference (in terms of the SHG response) between the bilayer structure described here and the previously addressed (001) monolayer can be detected.

We now turn to the (110) surface (Fig. 4), which, in the paramagnetic phase, reveals a lower symmetry than the (001) surface. On the other hand, the number of symmetry operations in the AF configurations is comparable to the (001) surface. In addition, as shown in Table IV, the resulting SHG response types are not very characteristic, so the detection possibilities for this surface are very limited. In particular, confs. (a) , (b) , (c) , (g) , (h) , (i) , (j) , (k) , and (l) give the same tensor elements as the paramagnetic phase. Confs. (d) , (e) , (f) , and “ferro3” bring new tensor elements. Other ferromagnetic configurations (“ferro1” and “ferro2”) present different sets of new tensor elements, making these configurations distinguishable from the others as well as from each other. Conf. “ferro4” yields a completely different set of tensor elements, however this set is related to the one of conf. “ferro1” by 90° rotation.

The study of the (111) surface (see Fig. 5) has to be separated in two subcases, according to whether we take into account only one atomic monolayer or more. In both subcases, we consider the same configurations. The SHG response types for the first subcase are listed in Table V, and for the second subcase in Table VI. For the *first* subcase, confs. (a) , (i) , and (k) reveal the same tensor elements as the paramagnetic phase, however due to the lower symmetry their values are not related to each other. Configurations (c) and (f) present new tensor elements. As for the previous surfaces, the ferromagnetic phase reveals completely different sets of tensor elements, and the three ferromagnetic configurations can be distinguished from each other since they bring different tensor elements into play. Unlike for the (110) surface, the axes x and y are not topologically equivalent, and thus the fact that tensor elements of “ferro1” are related to those of “ferro3” by 90° rotation does not affect the possibility to distinguish these two configurations. The ferromagnetic conf. “ferro5” brings up the same tensor elements as AF confs. (c) and (f) , but the relations between the elements are different. The *second* subcase (more layers taken into account) gives different sets of allowed tensor elements (compared to the first subcase) for each but the “ferro3” configuration. Confs. (a) , (i) , (k) , and “ferro3” share the same set of allowed tensor elements and can be easily distinguished from the paramagnetic phase. Confs. (c) , (f) , and “ferro1” reveal all tensor elements, with their values unrelated. Similarly, conf. “ferro5” presents another, distinguishable set of tensor elements. The possibility to distinguish the magnetic phases is rather limited.

The symmetry analysis of nonvanishing tensor elements for ferromagnetic surfaces in the case A have been performed by Pan *et. al.* [10]. Our analysis yields the same results, taking into account the corrections made

by Hübner and Bennemann [40].

B. Distortions of monoatomic lattice

The rhombohedral distortion of the atomic lattice, described here and shown in Fig. 6, makes the x and y axes of the (001) surface inequivalent, even in the paramagnetic phase. On the (111) surface, the y axis is not equivalent any longer to other axes connecting the nearest neighbors, namely $S_{(xy)}$ and $S_{(-xy)}$ (for the definition of the “S” and “H” axes see Fig. 5, the paramagnetic conf.). These inequivalences of axes are the reasons for the reduction of the number of symmetry operations in the paramagnetic phase. Because of this reduction some spin structures that previously formed different domains of a single configuration now cannot be transformed into each other and become “independent” configurations. This happens for almost every of the previously addressed configurations of the (001) and (111) surfaces. Consequently, all the depicted spin structures are in fact configurations, and are addressed in this subsection.

The resulting SHG response types for the (001) surface are listed in Table VII. For this surface, only two of the ferromagnetic configurations, namely “ferro1” and “ferro2” can be easily distinguished from both the paramagnetic as well as the antiferromagnetic phases. These ferromagnetic configurations can be also distinguished from each other. On the contrary, all the AF configurations yield only two types of response, and in addition one of them is equivalent to the response of the paramagnetic phase. Consequently, it will not be possible to determine the surface spin structure, and the distinction of the AF phase from the paramagnetic one can be successfully performed only in confs. a)-h) and o). Compared to the case A, there is an important symmetry breaking for most configurations. Thus, the distinction between the two cases (A and B) is possible (compare Tabs. II and VII).

All the (110) surfaces of an fcc crystal with a rhombohedral distortion are topographically equivalent to the (110) surface of the case A. The distortion only stretches the x or y axis, so the structure remains rectangular.

The analysis of the (111) surface (depicted in Fig. 6) in the subcase of only one monolayer reveals sets of symmetries very similar to the (110) surface, as it follows from the Table VIII. In fact, the (111) surface of a fcc crystal with a rhombohedral distortion can be treated as two rectangular lattices superimposed on each other. In turn, due to the distortion, it is not convenient any longer to describe the spin structures using “S” and “H” axes. The possibility to distinguish AF configurations is very poor, and two of the AF configurations (a) and k)) yield the same signal as the paramagnetic surface. In

confs. b) - j), l), and m) the AF phase can be distinguished from the paramagnetic one, but they give the same signal as conf “ferro5”. Conf. “ferro2” can be easily distinguished since it reveals a characteristic set of (all) tensor elements. Confs. “ferro1” and “ferro3” yield different sets of tensor elements, but they are related to each other by 90° rotation. Most of the configurations allow for the distinction of the cases A and B (compare Tabs. V and VIII).

In the subcase of two monolayers of the (111) surface, the symmetry is dramatically reduced (see Tab. IX). Even in the paramagnetic phase the group of symmetries consists of only one nontrivial operation, and this appears to occur also in the AF configurations a), i), k), and “ferro3”. In all the other configurations all tensor elements are allowed due to the lack of any symmetry. Only confs. paramagnetic and “ferro5” allow for the unambiguous distinction of the cases A and B (compare Tabs. VI and IX). Consequently, this surface is not very useful to an analysis of the magnetic structure, with the exception of stating the distortion itself.

As the conclusion of the case of the distorted sublattice of magnetic atoms, the surfaces give extremely limited possibilities to investigate the magnetic properties. In our further study, we will limit ourselves to lattices of undistorted magnetic atoms.

C. Structure with nonequivalent magnetic atoms

We assume now that not all the magnetic atoms in the cell are equivalent. An example of such a structure is a material composed of two magnetic elements, but also a situation when the magnetic lattice sites are inequivalent due to different bonds to a nonmagnetic sublattice; distortions of the sublattice of nonmagnetic atoms that preserve the center of twodimensional inversion produce the same effect. Other distortions of the sublattice of nonmagnetic atoms will be discussed in subsection D. The magnetic moment at the distinguished positions can be changed or not - this does not affect the results obtained by symmetry analysis. The configurations considered here are “ferro1”, “ferro2”, “ferro4”, a), b), c), e), f), i), k), m), o), p), and r) for the (001) surface (see Fig. 1), “ferro1”, ferro3”, “ferro5”, a), c), f), i), and k) for the (111) surface (see Fig. 5), and all configurations depicted in Fig. 4 for the (110) surface. Other depicted spin structures form domains of these configurations and are not referred to in this subsection nor in the tables concerning the current subsection.

The structure is depicted in Fig. 7. For the sake of brevity, we show the structure of the distinguished atoms only for the paramagnetic phase. All the configurations are the same as in case A, for all surface orientations. The already mentioned “convention” of alternating (or

not) spin directions along certain axes is applied regardless of the atom type. This allows us to obtain the whole crystal surface from the small displayed fragment.

Our analysis starts with the (001) surface of an fcc crystal. The SHG response types for each configuration are listed in Table X. In general, we can observe seven types of response. The first of them is represented by the paramagnetic phase alone. The second type of response, exhibited by the ferromagnetic “ferro1” and the AF a), b), e), o) confs., differs from any other type by some tensor elements. The confs. a) and o) reveal different tensor elements than the other configurations from the mentioned group. However, the signal from confs. a) and o) is the same as for the confs. b), e), and “ferro1” if one exchanges the axes x and y . Thus, if the directions of the spins cannot be determined by another method, confs. a) and o) cannot be distinguished from b), e), and “ferro1”. The next type consists of conf. f) and reveals all tensor elements, while no relations between them are enforced by the symmetry analysis. A completely different type of response is presented by conf. c) alone. Another type, where confs. i), m) and p) belong to brings the same tensor elements as conf. c), but there exist more relations between the elements due to a higher symmetry in these configurations. The next type is given by confs. “ferro2” and k). As in conf. f) all the tensor elements are present but this time there are some relations between them. In addition, confs. r) and “ferro4” yield a completely new set of tensor elements due to the preserved fourfold rotational symmetry.

Thus, assuming one atom as distinguished may reduce the symmetry. New tensor elements appear in confs. a), b), e), f), k), o), and r) compared to case A (compare Tabs. II and X). In these configurations it is therefore possible to distinguish the cases of equivalent and nonequivalent magnetic atoms, provided the tensor elements that make the cases different can be singled out by the experimental geometry. There exists also a possibility to distinguish different AF configurations in case C. The antiferromagnetic *phase* can be undoubtedly detected in the surface configurations c), f), i), m), and p).

For the (110) surface, there are more possibilities to distinguish the configurations with nonequivalent magnetic atoms than in the case A. However, the configurations still produce ambiguous signals (see Tab. XI). Confs. b), c), h), i), k), and l) are equivalent to the paramagnetic phase. Conf. a) is equivalent to the ferromagnetic “ferro1” configuration, and conf. d) to “ferro2”. In addition, the confs. e), f), and g) are equivalent to the conf. “ferro3” and conf. j) gives the same signal as conf. “ferro4”. Even the presence of nonequivalent atomic sites in the lattice cannot be detected by SHG on this surface, since the symmetry of the (110) surface is usually not lowered further by the existence of equivalent magnetic sites (compare Tables IV and XI. The only exception are

the confs. a), d), g), and j) which give different tensor elements in the two cases. As in the case of equivalent atoms, the (110) surface is not very useful for the analysis.

The study of the (111) surface must again be divided in the two subcases of one or more monolayers, respectively. Fig. 7 depicts the situation in the paramagnetic phase. The SHG response types are listed in Tables XII and XIII for the first and the second subcase respectively.

In the first subcase (one monolayer) the symmetry establishes six different types of nonlinear response. The “paramagnetic” type (for the paramagnetic configuration only) is characteristic - all the other configurations have additional tensor elements. The next type of response (the ferromagnetic conf. “ferro1” and the antiferromagnetic conf. a)) brings some new tensor elements. Other tensor elements appear in the conf. k). Configurations “ferro3” and i) show another set of nonvanishing tensor elements. The confs. c) and f) reveal all tensor elements in an unrelated way. In addition, conf. “ferro5” presents a characteristic set of tensor elements.

In the second subcase, only four different SHG responses are possible. Firstly, the paramagnetic phase is characteristic - all the other configurations bring additional tensor elements into play. The next type of response is presented by confs. “ferro3” and i) - they yield some additional tensor elements. Confs. “ferro1”, a), c), f), and k) reveal all tensor elements and no relations between them appear from our symmetry analysis. Again, the conf. “ferro5” presents a unique set of nonvanishing tensor elements.

Consequently, for the (111) surface, the symmetry breaking due to the presence of a second kind of magnetic atoms has even more important consequences than for the (001) surface. In the situation of only one monolayer, the distinction between the cases may be possible for all the AF configurations (compare Tables V and XII). Considering additional layers leads to further symmetry breaking and renders the distinction between the configurations impossible. The distinction between the cases A and C is possible in confs. a) and k) (compare Tables VI and XIII). Besides, in most configurations it is possible to decide if these additional layers play any role (compare Tables XII and XIII).

D. Distorted oxygen sublattice

Due to the strong charge-transfer between nickel and oxygen in NiO the sublattices may be distorted. This effect can lower the symmetry of the surface. A point-charge model calculation by Iguchi and Nakatsugawa [41] presented a shift of the oxygen sublattice (“rumpling”) in the direction perpendicular to the surface. Their method did not show any in-plane displacement and thus no change of the surface symmetry. However, if the “rumpling”

also has an in-plane component, i.e. if the oxygen atoms are displaced also in the x and y directions, it will also have a considerable effect on the symmetry of the crystal surface. For this paper, we have chosen a distortion that can lower the symmetry of the surface and besides that can lower the symmetry of the surface and besides that can be represented within one conventional unit cell. The configurations considered here are “ferro1”, “ferro2”, “ferro4”, a), b), c), e), f), i), k), m), o), p), and r) for the (001) surface (see Fig. 1), “ferro1”, ferro3”, “ferro5”, a), c), f), i), and k) for the (111) surface (see Fig. 5), and all configurations depicted in Fig. 4 for the (110) surface. Other depicted spin structures form domains of these configurations and are not referred to in this subsection nor in the tables concerning the current subsection.

As will be shown later, the best conditions for the detection of this kind of distortion are presented by the (110) surface. The (111) surface could show equally good possibilities if only a monolayer of magnetic atoms is present.

In the presence of an oxygen sublattice distortion, the chemical unit cell is also doubled. This effectively means that magnetic unit-cell-doubling (describing the fact that the magnetic unit cell is twice as big as the chemical one) is lifted. In general, taking into account distorted oxygen atoms in the paramagnetic phase does not lower the symmetry of the problem. The exception is the (111) surface, where the six-fold axis is replaced by the three-fold one.

In the case of the distorted oxygen sublattice, the symmetry group for each configuration is a subgroup of the corresponding “non-distorted” configuration, i.e. of the corresponding spin configuration in the case where the oxygen atoms are not considered. As in case C we display only the paramagnetic phase in Fig. 8 to depict the atom positions. All the spin configurations are the same as for the corresponding surfaces in case A, and the spins are assumed to be equivalent.

As Table XIV shows, six different responses can be expected from the (001) surface. The paramagnetic surface will give a characteristic response. The second group is formed by the confs.: a), b), e), o), and “ferro1”. Although confs. a) and o) have elements different from the remaining configurations in this group, this fact corresponds simply to rotating the sample by 90° with respect to the z axis. Confs. c) and f) reveal all tensor elements without relations between them. Confs. “ferro2”, i), k), and m) reveal all tensor elements with some relations. The only difference between conf. m) and others from this group is like for the previous group a 90° rotation with respect to the z axis. Another group consists of conf. p) alone. It reveals the same tensor elements as the paramagnetic phase, but certain relations between tensor elements are broken due to a lower symmetry of the conf. p). The confs. r) and “ferro3” form the last group. All the configurations but k) and “ferro3” can be distinguished from those of case A (compare Tabs. II and XIV). However only confs. c) and g) can be distin-

guished from case C (compare Tabs. X and XIV). Thus, only in these configurations it will be possible to detect oxygen sublattice distortions by SHG.

The SHG response types for the (110) surface are presented in Table XV. One can observe that only configurations c), f) and i) give rise to new (compared to case A, Table IV) tensor elements. Compared to case C (Table XI), confs. c), f), and i) bring new tensor elements, and, surprisingly, confs. a) and g) have less tensor elements, due to higher symmetries in the case D. Consequently, the confs. a), c), f), g), and i) allow for an unambiguous determination of the oxygen sublattice distortion from the (110) surface. The possibility to distinguish different configurations is rather limited.

Oxygen sublattice distortion similar to the one presented in Fig. 8 for a (111) surface was found by Renaud *et al.* [42] and calculated by Gillan [43] in M_2O_3 materials ($M = Al, Fe$). Since the nonmagnetic sublattice symmetry group has an influence on SHG this distortion can be detected also on surfaces of fcc crystals. In the previous cases A and C we divided the study of (111) surfaces in two subcases, considering either one or more atomic layers. Taking into account a distorted oxygen sublattice leads us immediately to the subcase of “more atomic layers”. It is caused by the fact that the oxygen and magnetic atoms belong to mutually exclusive planes. The resulting SHG response types are listed in Table XVI. For the AF and ferromagnetic phases, all tensor elements are allowed for every configuration. Thus SHG cannot detect the magnetic phase of the surface nor distinguish different configurations. Only confs. paramagnetic, “ferro3”, “ferro5”, and d) allow to decide unambiguously whether the oxygen sublattice is distorted or not (compare Tabs. VI, XIII, and XVI).

For both the (001) and (111) surfaces, the symmetry groups of case D appear to be the subgroups of the corresponding configurations of case C. This means that the oxygen sublattice distortion makes some (one half of all) magnetic atoms distinguished as in case C, even though we did not apply this distinction explicitly in case D. On the other hand, the symmetry groups of the case D differ essentially from those of case B. This is caused by the difference in distortions assumed in these cases: the rhombohedral one in case B and rotation-like in case D.

E. Domain imaging

For simplicity, we will consider here only surfaces described hitherto by the case A of our analysis. In this case, for AF surfaces, no 180° domains can be expected due to the presence of magnetic unit-cell doubling. The allowed domains can be detected by surface-sensitive SHG under the following two conditions.

First, domains can be imaged by our method only if they manifest themselves at the surface, i.e. if the surface

spin ordering changes while passing from one domain to another [44]. It is necessary to note, however, that the spin orderings for different domains must belong to the same *configuration* in the sense of our classification. We do not consider it as a domain structure if one portion of the surface is in one configuration and another portion is in a different configuration. Under such conditions, we can encounter two different types of domains: 90° domains (for the (111) surface they are rather 60° domains), resulting from the rotations around z axis, and the second type (called by us mirror-domains, characteristic for antiferromagnets), where spins point along the same axis in all domains, but the ordering is still different (they are no 180° domains!). The tables contain the complete information about the parity of tensor elements in mirror-domain operations, and also for 90° type domains, but not for 60° domains. The 90° type domains will be addressed later on. In the mirror-domain structure, the magnetic point group describing the configuration must lack an operation that, while belonging to the (nonmagnetic) point group of the system *and* leaving the spin axes invariant, only flips some of the spins. Note, the flipped subset of the spins must be antiferromagnetically ordered in itself. Configurations, the symmetry groups of which *lack* one of these operations can reveal surface domains, related to each other by this operation.

For an illustration we choose the configuration c) of the (001) surface (see Fig. 1). The spins point along the x axis. Thus operations leaving the axis invariant are $\bar{2}_x$, $\bar{2}_y$ and 2_z . Of them, $\bar{2}_x$ and $\bar{2}_y$ are absent in the magnetic point group of the considered configuration (see Tab. II, conf. c), and Tab. I). The flipped subset of spins consists of the four outer spins for the $\bar{2}_x$ operation, and of the central spin for $\bar{2}_y$ (see Fig. 9 b) and c), respectively). In fact, there are two domains possible in this configuration: one with the spins kept invariant under translations by the vector $(-\frac{a}{2}, \frac{a}{2}, 0)$ (this domain is shown) and the other with the spins kept invariant under translations by the vector $(\frac{a}{2}, \frac{a}{2}, 0)$. Here, a denotes the lattice constant. These domains are depicted in Fig. 9.

The second condition for domain imaging is an interference. It can be created internally by different elements of the tensor $\chi^{(2\omega)}$ or by external reference [45,46]. The interfering elements should be of a similar magnitude for the largest possible image contrast. Group theory, however cannot account for the amplitudes. With external as well as internal reference, a tensor element that changes its sign under the reversal of the antiferromagnetic order parameter \mathbf{L} is necessary. Actually, every \mathbf{L} dependence of $\chi^{(2\omega)}$ can be represented by splitting the tensor elements into odd and even ones in \mathbf{L} ; even if a tensor element is not purely odd or even we can always decompose it according to:

$$\chi_{ijk}^{(2\omega)} = \chi_{ijk}^{(2\omega),odd} + \chi_{ijk}^{(2\omega),even} \quad (5)$$

i.e. a tensor element consists of parts which are odd and

even in \mathbf{L} , respectively. In a system with many terms of that kind the possibility of detecting domains may be limited, since they can influence the signal with opposite sign, thus diminishing the interference. In highly symmetric structures, such as an fcc crystal, the situation is more comfortable: every tensor element is either odd or even in \mathbf{L} (see Appendix). By the appropriate set of experiments an element can be singled out and give a clear image of AF domains.

As an example we consider tensor elements that are present in all the phases, e.g. $\chi_{zzz}^{(2\omega)}$: they are even in the magnetic order parameters \mathbf{L} and \mathbf{M} , for the AF and ferromagnetic phases, respectively. The tensor element $\chi_{zxy}^{(2\omega)}$, present for example in the previously discussed conf c) of the (001) surface (see Fig. 9), is odd, since it changes its sign under the operation $\bar{2}_x$ transforming one domain into another. For other configurations other tensor elements and operations can be found. In the discussed configuration both these elements are present, we have intensity contributions proportional to $(\chi_{zzz}^{(2\omega)})^2$, $(\chi_{zxy}^{(2\omega)})^2$ and $\chi_{zzz}^{(2\omega)} \cdot \chi_{zxy}^{(2\omega)}$, due to the square in Eq. (2). As a result, one obtains an interference:

$$I_p \sim \dots + (\chi_{zzz}^{(2\omega)})^2 + (\chi_{zxy}^{(2\omega)})^2 \pm 2\chi_{zzz}^{(2\omega)} \cdot \chi_{zxy}^{(2\omega)} + \dots \quad (6)$$

where “+” stands for one domain, “-” for a different one.

Now, we turn to the 90° domain structure. Again, we take the conf. c) of the (001) surface as an example. The operation connecting the domains is 4_z . Under this operation, the tensor element $\chi_{zxy}^{(2\omega)}$ changes its sign, thus again we have an interference which renders the domain imaging possible. This tensor element is even in the domain operation $\bar{2}_{xy}$ (which is equivalent to the superposition of $\bar{2}_x$ and 4_z), which means that domains related to each other by this operation cannot be imaged using this particular tensor element. Similarly, if a tensor element is odd in one domain operation and even in another, it must be odd in their superposition. Concerning the 60° domains for (111) surfaces, the parity of the tensor elements must be treated more carefully, as indicated already in [36]. We can still define three “twofold” operations, and each of them has its own set of odd and even tensor elements. The sets corresponding to different of those operations are not mutually exclusive, i.e. a tensor element is usually shared among different parities. In this way, this tensor can be positive in one domain, negative in the second, and zero in the third one. Thus, the existence of a well defined parity of tensor elements is necessary for domain imaging, but not sufficient for 60° and 120° domain structure.

This unleashes an interesting question of the antiferromagnetic order parameter. There are as many order parameters as different domain structures for a given configuration. For 60° and 120° domain structures, the AF

order parameter must be a vector, while for mirror domains it is a number. For 90° domains it can be also a number, since there are only *two* 90° domains. The vectorial order parameter transforms itself under the domain operation like a usual vector.

It is necessary to mention at this point that taking into account the spin structure in the *second layer* would not change the validity of the analysis presented in this subsection. The only modifications would result from addressing bulk domains rather than surface domains, and the symmetry of the AF configurations would be changed. Yet it would still be possible to find domain operations as well as odd and even tensor elements leading to interference and AF domain contrast. However the possibility to identify each of the domains may be limited in some cases due to the increased number of domains.

IV. POSSIBLE EXPERIMENTAL SETUPS

In this section, we propose and discuss possible experimental setups for the detection of AF configuration and the imaging of AF domains from low-index surfaces of NiO that exhibit magnetic unit-cell doubling in contrast to bulk Cr_2O_3 [1,21]. We propose an experimental setup for the *detection* of antiferromagnetism in the following way: both the incident and reflected beams may lie in the xz plane (optical plane), and form the angle ϑ with the z -axis (normal to the sample surface). In the plane perpendicular to the outgoing beam axis, the electric field of the second-harmonic generated light has two components, $E_p^{(2\omega)}$ and $E_s^{(2\omega)}$, given by the formulae

$$\begin{aligned} |E_p^{(2\omega)}| &= |\cos \vartheta E_x^{(2\omega)} - \sin \vartheta E_z^{(2\omega)}| \\ |E_s^{(2\omega)}| &= |E_y^{(2\omega)}| \end{aligned} \quad (7)$$

$E_x^{(2\omega)}$, $E_y^{(2\omega)}$, and $E_z^{(2\omega)}$ are the components of the electric field resulting from SHG in the coordinate system of the sample. The dependence of these components on the input electric field is indicated by the tensor $\chi^{(2\omega)}$. The aim of the experiment is the determination of vanishing and nonvanishing tensor elements. The easiest way to do this is to analyze the output signal intensity as a function of the input polarization in both output polarizations s and p , for a fixed angle of incidence and reflection. The dependence of the output second-harmonic electric field on the input polarization is schematically displayed in Fig. 10a)-c) for all tensor elements. The intensity of SHG light is the square of the linear combination of these partial responses. An example of the intensity dependence on the input polarization is presented in Fig. 10d). The intensity need not be symmetric with respect to $\varphi = 90^\circ$, this results from the influence of the electric field depicted in Fig. 10c). The coefficients of the mentioned combination are the products of the $\chi^{(2\omega)}$ tensor elements and the

corresponding Fresnel coefficients, according to Eq. (2). Thus performing a best fit of these coefficients to the experimental results will give (after taking into account the Fresnel and geometrical coefficients, known for the given experimental geometry and material [35]) a set of nonvanishing elements of the $\chi^{(2\omega)}$ tensor. Thus for instance, the magnetic phase can be determined.

Concerning another experimental geometry, with input polarization fixed and intensity measured as a function of the output polarization, it is possible to determine whether the nonlinear Kerr effect takes place. For instance, with the input polarization $\varphi = 90^\circ$, the output electric field is given as follows [35]:

$$\begin{aligned} E^{(2\omega)} &= \sin \Phi (A_2(\Theta) \chi_{yyy}^{(2\omega)} B_2(\vartheta)) + \\ &\cos \Phi (A_1(\Theta) \chi_{xyy}^{(2\omega)} B_2(\vartheta) + A_3(\Theta) \chi_{zyy}^{(2\omega)} B_2(\vartheta)) \end{aligned} \quad (8)$$

As the result, maximum of the intensity is for $\Phi \neq 90^\circ$, if at least one of the tensor elements $\chi_{xyy}^{(2\omega)}$ or $\chi_{zyy}^{(2\omega)}$ does not vanish. Actually, tensor element $\chi_{zyy}^{(2\omega)}$ is even in all the investigated order parameters, but the tensor element $\chi_{xyy}^{(2\omega)}$ can be odd. For such configurations the Kerr effect (change of polarization caused by inversion of the magnetic order parameter) takes place. Thus, it is possible to determine which tensor elements are associated with the spin-orbit coupling.

The geometry with p polarization of the reflected SHG light seems to be less useful, since there the tensor element $\chi_{zzz}^{(2\omega)}$ is always present, regardless of the configuration. Besides, this polarization mixes the $\chi_{x..}^{(2\omega)}$ and $\chi_{z..}^{(2\omega)}$ tensor elements. This mixing, however, can be tuned by varying the angle of incidence ϑ and taking into account the influence of the Fresnel coefficients. For smaller ϑ only the $\chi_{x..}^{(2\omega)}$ elements are important, while for larger ϑ the $\chi_{z..}^{(2\omega)}$ dominate. If the experiment does not show any difference for these two situations, the tensor elements must be related. This is the possibility to distinguish the configurations with some relations between the tensor elements from those without such relations. On the other hand, the p polarization is useful for AF domain *imaging*. Thus one of the experimental possibilities is to carry out the measurements first in s polarized outgoing SHG light to make sure that the material is in the AF phase and determine its spin configuration. Then a second measurement in p polarization can be performed for the domain imaging.

V. CONCLUSIONS

Already a short look at the presented tables shows that our method works best if the paramagnetic phase is of high symmetry, since then a wide variety of different symmetries exists which may be broken by different spin configurations. In other words, there is enough room for different new tensor elements to appear along with different

spin ordering under these circumstances. In general, this is the main reason why only nonlinear optics is suited for the detection of antiferromagnetism and the imaging of AF domains. The linear susceptibility tensor has too low a number of elements for these purposes in order to produce unambiguous results. Similarly, among the considered surfaces, the (110) surface is the least useful for the analysis as it yields ambiguous signal interpretations due to its low symmetry in the paramagnetic phase, and, on the other hand, very similar symmetries in all the AF configurations.

The (001) and (111) surfaces present alike possibilities of distinction between the cases. If more than one monolayer is involved, however, the (111) surface will give the same response in the cases A (all atoms equivalent) and C (two kinds of magnetic atoms). Both the (001) and (111) surfaces also allow for the determination of the spin structure, provided the case is known. The (111) surface in the case D (oxygen sublattice distortion) is an exception - all the AF configurations produce the same response. It is possible, however, to determine the phase of the material.

The case D appears to be a subgroup of the case C, i.e. all the magnetic point groups describing the configurations of the case D are subgroups of the corresponding ones in the case C. The only exception is the (110) surface. This inclusion means that the oxygen sublattice distortion makes some (one half of all) magnetic atoms distinguished as in case C, even though we did not apply this distinction explicitly in case D.

From the fact, that the influence of oxygen sublattice distortion (case D) is not detectable in the paramagnetic and ferromagnetic phases it follows that only antiferromagnetic ordering can give an extensive information about the structure of the surface. It is the magnetic atoms and their magnetism which reveal the presence and position of oxygen.

Our short analysis of an AF bilayer structure (surface (001)) indicates very similar features to the (001) monolayer. There exists a possibility to distinguish AF configurations from each other, and a certain possibility to detect the magnetic phases. Furthermore, introducing the second atomic layer does not affect the possibility to image AF domains.

Concerning the *magnetic* phases, configurations and cases considered in this paper, some *a priori* information about the *structure* is needed in order to draw unique conclusions from the experimental results. For the detection of the phase and the spin configuration this additional information is the case (A, B, C, D). Vice versa, the case (for instance a possible distortion of the oxygen sublattice) can be determined if one knows the configuration (and if it had been previously deduced that the investigated material is antiferromagnetic). Actually, in most measurements of AF spin structures some *a priori* knowledge is required. For example, in experiments by Fiebig

et. al. [21] such a prerequisite is the assumption of the AF spin-flop phase of the material. In both experimental approaches mentioned here the (001) surface seems to provide the best possibilities of drawing valuable conclusions, while the (110) surface is the least suitable in that respect.

Finally, our paper demonstrates that the AF domain imaging is possible even in the presence of magnetic unit-cell doubling. Thus optical SHG, unlike linear optics, is able to image AF *surface* domains. For most AF configurations, there are more than one surface domain structures. The rule stating that the number of domains is equal to the number of symmetry operations in the paramagnetic phase divided by the number of symmetry operations in the magnetic phase is applicable also for antiferromagnets (thus, with unit-cell doubling the number of domains is reduced by a half). However, not all the domains can be imaged at the same time.

APPENDIX ON THE GROUP-THEORETICAL ANALYSIS OF MAGNETIC SYSTEMS

In this Appendix, we would like to address some particularities of our group-theoretical analysis. The first general remark is that although symmetry analysis can provide us with a set of nonvanishing tensor elements for a given configuration, but cannot give any information about their magnitude. This equally applies to the distortion effects, as treated e.g. in Ref. [29].

Another interesting issue is the behavior of the tensor elements with respect to the AF order parameter \mathbf{L} (for ferromagnetic phases \mathbf{L} should be replaced by the magnetization \mathbf{M}), i.e. the parity of tensor elements. In general, a tensor element consists of even and odd parts with respect to \mathbf{L} , as shown in Eq. (5). In systems with high symmetry, it is possible to describe an operation which reverses \mathbf{L} (or \mathbf{M}) by a spatial operation \hat{l} . The operation \hat{l} belongs to the point group of the system, but not to its magnetic point group. The application of this operation to a tensor element will change its sign (keep it invariant) if this element is odd (even) in \mathbf{L} . Consequently, each tensor element can be either odd or even in \mathbf{L} , a mixed behavior is forbidden. Actually, the parity of a given tensor element is a function of the chosen operation \hat{l} . In most antiferromagnetic configurations more than one operation leading to different domain structures are possible (this means, more than one order parameter can be defined). For example, for (001) surface one has 4_z rotations leading to different domains *in addition* to the eventual mirror-structure. For the (111) surface, there are three domains resulting from the rotations with respect to the z axis alone. For some configurations, they exist in addition to the mirror-domains.

This whole analysis of the parity of the tensor elements cannot be performed for the systems with a lower symmetry, where it is impossible to find an operation \hat{l} describing the inversion of \mathbf{L} or \mathbf{M} , a mixed behavior is then allowed. Note, the presence of dissipation (redistribution of response frequencies) does not influence the above consideration. In general, dissipation in frequency space is responsible for the mixing of the real and imaginary parts in the tensor elements, while point-group symmetry governs the (non)existence of tensor elements purely odd or even in the magnetic order parameters \mathbf{L} or \mathbf{M} .

We acknowledge financial support by TMR network through NOMOKE contract no. FMRX-CT96-0015. We also acknowledge numerous fruitful discussions with Dr. R. Vollmer.

-
- [1] M. Fiebig, D. Fröhlich, B. B. Krichevtsov, and R. V. Pisarev, Phys. Rev. Lett. **73**, 2127 (1994).
- [2] P. Argryes, Phys. Rev. **97**, 334 (1955).
- [3] W. L. Roth, J. Appl. Phys. **31**, 2000 (1960).
- [4] V. V. Eremenko and N. F. Kharchenko, Sov. Sci. Rev. A **5**, 1 (1984).
- [5] J. F. Dillon, J. Magn. Magn. Mat. **100**, 425 (1991).
- [6] W. F. Brown, S. Shtrikman, and D. Treves, J. Appl. Phys. **34**, 1233 (1963).
- [7] V. V. Eremenko and N. F. Kharchenko, Phys. Rep. **155**, 379 (1987).
- [8] I. Dzyaloshinskii and E. V. Papamichail, Phys. Rev. Lett. **75**, 3004 (1995)
- [9] D. Fröhlich, Physica Scripta **T35**,125 (1995)
- [10] R. P. Pan, H. D. Wei, and Y. R. Shen, Phys. Rev. B **39**, 1229 (1989).
- [11] T. A. Luce, W. Hübner, and K. H. Bennemann, Phys. Rev. Lett. **77**, 2810 (1996).
- [12] A. Kirilyuk, T. Rasing, R. Mégy, and P. Beauvillain, Phys. Rev. Lett. **77**, 4608 (1996).
- [13] A. V. Petukhov, I. L. Lyubchanskii, and T. Rasing, Phys. Rev. B, **56**, 2680 (1997).
- [14] U. Pustogowa, T. A. Luce, W. Hübner, and K. H. Bennemann, J. Appl. Phys. **79**, 6177 (1996).
- [15] M. Straub, R. Vollmer, and J. Kirschner, Phys. Rev. Lett. **77**, 743 (1996).
- [16] S. A. Kutsenko, V. V. Lebedeva, and A. E. Sedelnikova, Opt. Spectrosc. (USSR) **68**, 684 (1990).
- [17] J. Schmalian and W. Hübner, Phys. Rev. B **53**, 11860 (1996).
- [18] K. B. Lyons, J. Kwo, J. F. Dillon, G. P. Espinosa, M. McGlashan-Powell, A. P. Ramirez, and L. F. Schneemeyer, Phys. Rev. Lett. **64**, 3294 (1990).
- [19] T. Rasing, M. Groot Koerkamp, and B. Koopmans, J. Appl. Phys. **79**, 6181 (1996).
- [20] S. Kielich and R. Zawodny, Acta Phys. Polonica A **43**, 579 (1973).
- [21] M. Fiebig, D. Fröhlich, and H-J. Thiele, Phys. Rev. B **54**, R12681 (1996).
- [22] M. Fiebig, D. Fröhlich, G. Sluiterman, and R.V. Pisarev, Appl. Phys. Lett. **66**, 2906 (1995).
- [23] S. Kielich and R. Zawodny, Optics Comm. **4**, 132 (1971).
- [24] I. L. Lyubchanskii, Phys. Solid State **37**, 387 (1995).
- [25] S. B. Borisov, N. N. Dadoenkova, I. L. Lyubchanskii, and V. L. Sobolev, Sov. Phys. Solid State **32**, 2127 (1990).
- [26] S. B. Borisov, N. N. Dadoenkova, I. L. Lyubchanskii, and V. L. Sobolev, Sov. Phys. Solid State **33**, 1061 (1991).
- [27] N. N. Akhmediev, S. B. Borisov, A. K. Zvezdin, I. L. Lyubchanskii, and Yu. V. Melikhov, Sov. Phys. Solid State **27**, 650 (1985).
- [28] V. N. Muthukumar, R. Valenti, and C. Gros, Phys. Rev. Lett. **75**, 2766 (1995).
- [29] Y. Tanabe, M. Muto, and E. Hanamura, Solid State Comm. **102**, 643 (1997).
- [30] The authors perform the analysis of $\chi^{(2\omega)}$ in the frequency space. There are no reasons to neglect the damping in this approach. On the contrary, if the dissipation is neglected, then, for instance, the Kramers-Kronig relations cannot be applied. In real time, on the other hand, the dissipation does not take place, as stated in [47].
- [31] M. Trzeciecki, W. Hübner, unpublished.
- [32] A. Dähn, W. Hübner, and K. H. Bennemann, Phys. Rev. Lett. **77**, 3929 (1996).
- [33] Symmetry properties of electromagnetic tensors can also explain other than optical effects, for example weak ferromagnetism of some AF materials was first qualitatively explained by means of symmetry theory (Dzyaloshinskii, Sov. Phys. **5**, 1259 (1957)).
- [34] R. R. Birss, *Symmetry and Magnetism* (North Holland, Amsterdam, 1964).
- [35] J. E. Sipe, D. J. Moss, and H. M. van Driel, Phys. Rev. B **35**, 1129 (1987).
- [36] The notion of the parity operation requires that the original situation is restored after applying the operation at most twice. Obviously, 2_z is such an operation, and for certain configurations 4_z satisfies this criterion as well (where 2_z is just a symmetry operation). However, neither 3_z nor 6_z have this property - they must be applied at least 3 times to restore the original situation. Concerning the tensor elements, for 2_z and mirror-operations a given tensor element may change its sign or not. Upon the application of the 4_z operation it may become another tensor element (i.e. its x indices become y and vice versa) while its sign can change or remain unchanged. Upon the 3_z operation, however, a single tensor element gets “split” into several tensor elements, and the notion of the conservation (or not) of the sign of the tensor element loses its sense. The tensor elements are described in the cartesian coordinate system, where quarters are the elementary entities. Rotation by an angle other than 90° and its multiples cannot be described as interchanging the axes and a possible modification of their signs. However, it is possible to treat the parity of tensor elements in the 3_z and 6_z operation in a more complicated way.
- [37] M. Trzeciecki and W. Hübner, Appl. Phys. B,**68**, 473 (1999).
- [38] If a spin structure is not described within this subsection (nor in the tables relevant to this subsection), it is a

- domain of the last displayed configuration that precedes the omitted one. This applies to all the subsections.
- [39] Although our primitive cell contains 4 magnetic atoms they are not placed on one line, and thus we still have a two-sublattice antiferromagnet.
 - [40] W. Hübner, K. H. Bennemann, Phys. Rev. B **52**, 13411 (1995).
 - [41] E. Iguchi and H. Nakatsugawa, Phys. Rev. B **51**, 10956 (1995).
 - [42] G. Renaud, B. Villette, I. Vilfan, and A. Bourret, Phys. Rev. Lett. **73**, 1825 (1994).
 - [43] M. J. Gillan, unpublished.
 - [44] It is also possible for different bulk domains to yield the same spin ordering at the surface.
 - [45] M. Fiebig, D. Fröhlich, and R.V. Pisarev, J. Appl. Phys. **81**, 4875 (1997)
 - [46] M. Fiebig, D. Fröhlich, S. Leute, and R.V. Pisarev, Appl. Phys. B. **66**, 265 (1998).
 - [47] F. Bassani and S. Scandolo, Phys. Rev. B **44**, 8446 (1991).
 - [48] A. Dähn, “Gruppentheorie der optischen Frequenzverdopplung an antiferromagnetischen Oberflächen”, Master’s Thesis, Freie Universität Berlin, 1996.

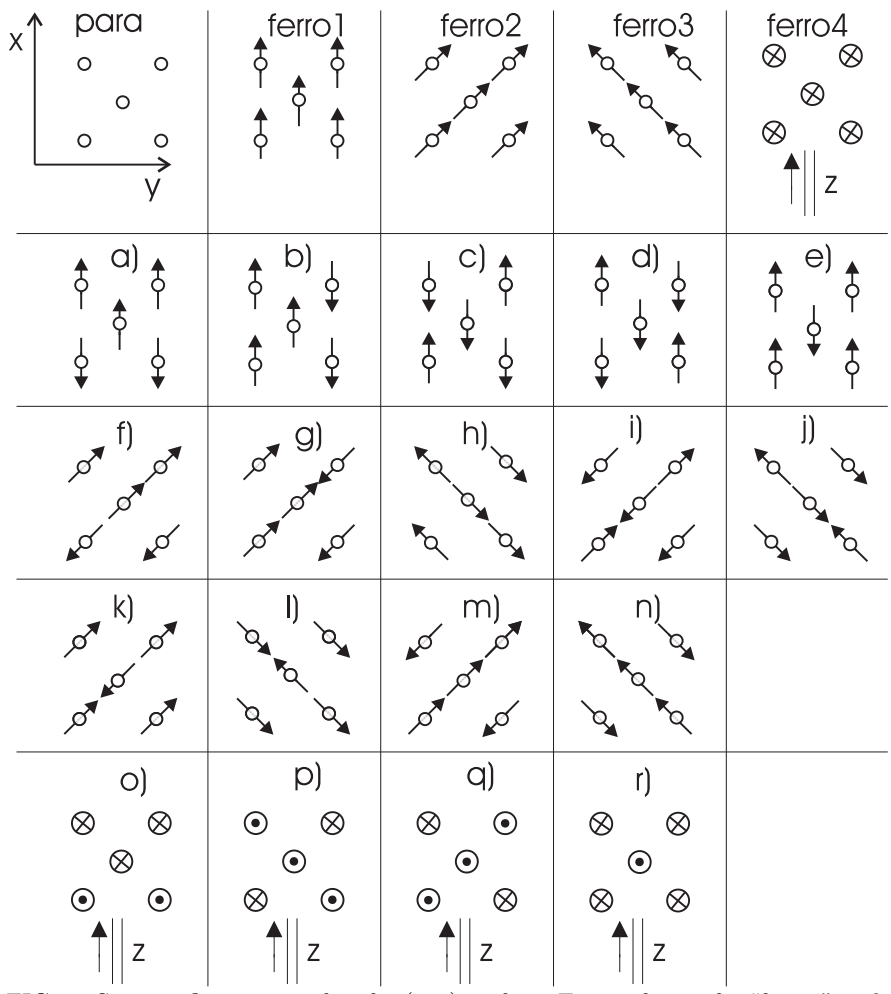


FIG. 1. Spin configurations of an fcc (001) surface. Except for confs. “ferro4” and o) - r), the arrows always indicate in-plane directions of the spins. In confs. “ferro4” and o) - r) \odot (\otimes) denote spins pointing along the positive (negative) z-direction, respectively.

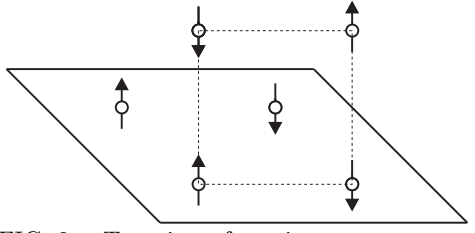


FIG. 2. Top view of a spin structure on a (001) surface. The dashed line depicts a conventional unit cell, while the solid one outlines the primitive unit cell.

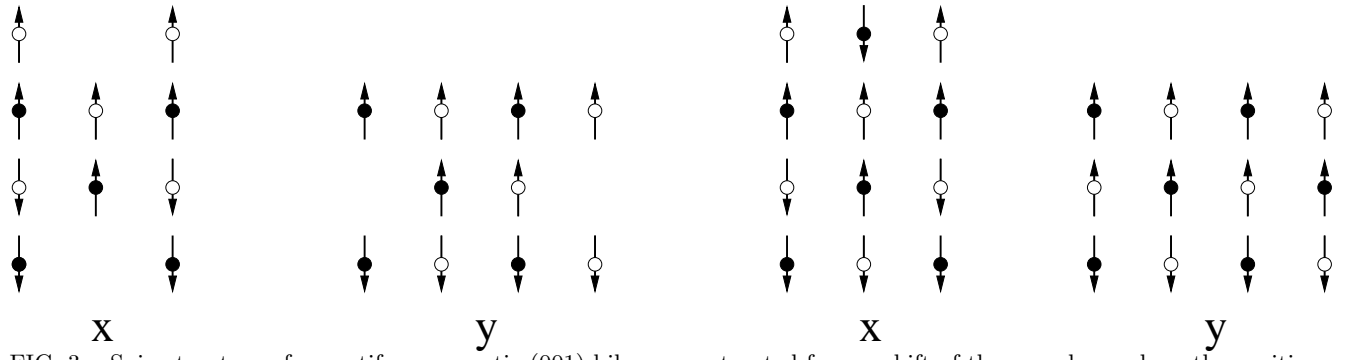


FIG. 3. Spin structure of an antiferromagnetic (001) bilayer constructed from a shift of the monolayer along the positive x (y) axis. Filled (empty) circles represent the topmost (second) layer. On the right hand side the conventional unit cells for the resulting bilayer structure are presented. Here, conf. a) of the (001) monolayer serves as an example.

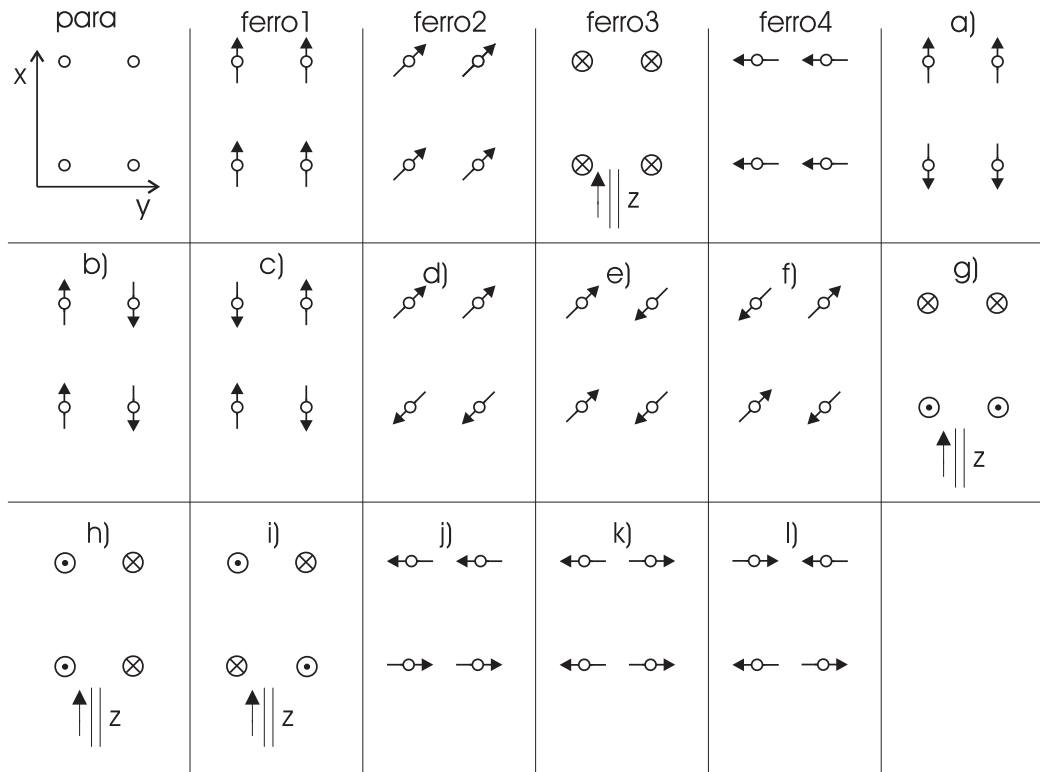


FIG. 4. Spin configurations of an fcc (110) surface. Except for confs. “ferro3”, g), h), and i), the arrows always indicate in-plane directions of the spins. In confs. “ferro3”, g), h), and i) \odot (\otimes) denote spins pointing along the positive (negative) z -direction, respectively.

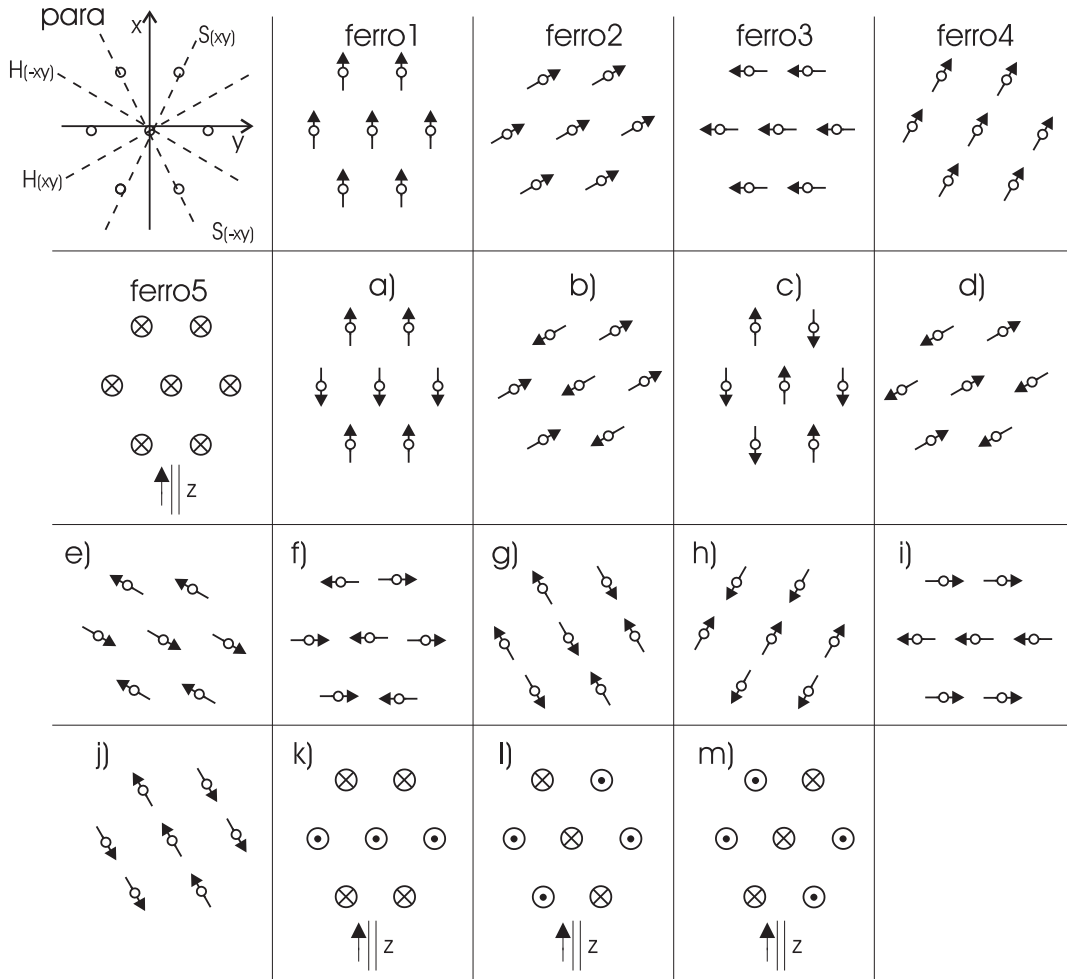


FIG. 5. Spin configurations of an fcc (111) surface. Except for confs. “ferro5”, k), l), and m), the arrows always indicate in-plane directions of the spins. In confs. “ferro5”, k), l), and m) \odot (\otimes) denote spins pointing along the positive (negative) z-direction, respectively.

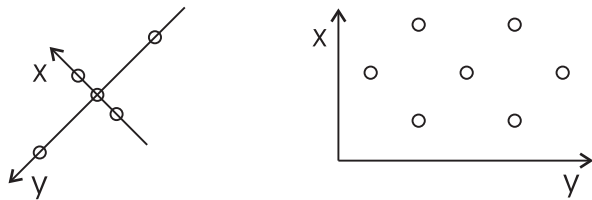


FIG. 6. Structure of the (001) and (111) surfaces of a fcc crystal with a rhombohedral distortion in the paramagnetic phase. Note the changed orientation of the coordinate system for the (001) surface.

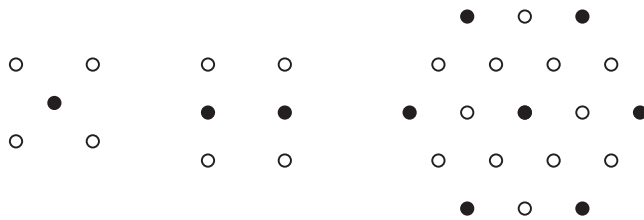


FIG. 7. Surface structure of the non-equivalent magnetic atoms case in the paramagnetic phase. Pictures present the (001), (110), and (111) surfaces, respectively. Filled and empty circles represent the two kinds of magnetic atoms. Note, the fragment representing the (111) surface does not show the conventional unit cell but a bigger set of atoms in order to give a clear idea about the surface structure.

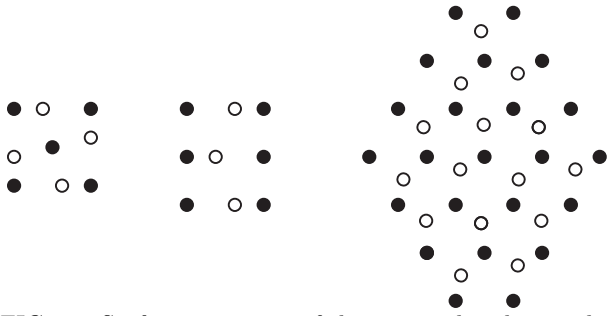


FIG. 8. Surface structures of the case with a distorted oxygen sublattice (white circles). Pictures present the paramagnetic phase of (001), (110), and (111) surfaces, respectively. Note, the fragment representing the (111) surface does not show the conventional unit cell but a bigger set of atoms in order to give a clear idea about the surface structure.

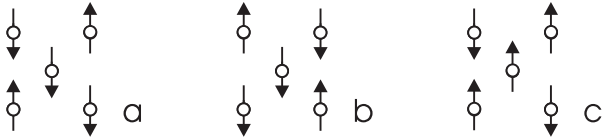


FIG. 9. Two surface mirror domains for an AF configuration - panels b) and c) depict the same AF domain, related to the panel a) by different mirror operations.

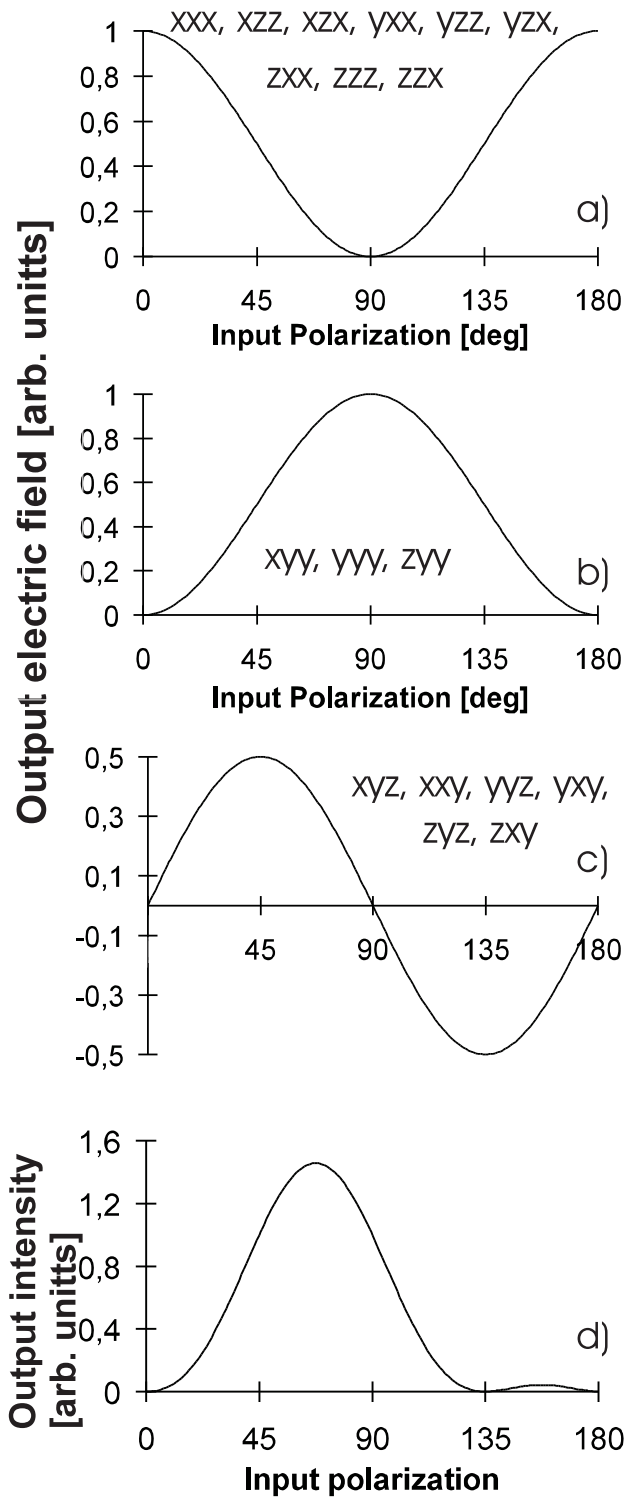


FIG. 10. Electric field response of single tensor elements as a function of the input polarization. Tensor element $\chi_{ijk}^{(2\omega)}$ is denoted as ijk . Graph d) shows an example of the SHG light intensity.

TABLE I. Details of SHG response types. We denote $\chi_{ijk}^{(2\omega)}$ by ijk . Odd elements are in bold if a domain operation exists.

key	point group	symmetry operations	domain operation	non-vanishing tensor elements
a	4mm	$1, 2_z, \pm 4_z, \bar{2}_x, \bar{2}_y, \bar{2}_{xy}, \bar{2}_{-xy}$	-	$xxz = xzx = yyz = yzy, zxx = zyy, zzz$
b	m	$1, \bar{2}_x$	$2_z, \bar{2}_y$	$xzx = xxz, \mathbf{xyy} = \mathbf{xyx}, \mathbf{yxx}, \mathbf{yyy}, \mathbf{yzz},$ $yyz = yzy, zxx, zyy, zzz, \mathbf{zyz} = \mathbf{zzy}$
c	m	$1, \bar{2}_{xy}$	$4_z, \bar{2}_{xy}$ $2_z, \bar{2}_{-xy}$ $4_z, \bar{2}_y$	no information about the parity $\mathbf{xxx} = \mathbf{-yyy}, \mathbf{xyy} = \mathbf{-yxx}, \mathbf{xzz} = \mathbf{-yzz},$ $xyz = yxz = xzy = yzx, xxz = xzx = yyz = yzy,$ $\mathbf{xxy} = \mathbf{-yyx} = \mathbf{xyx} = \mathbf{-yxy}, zxx = zyy, zzz,$ $\mathbf{zxx} = \mathbf{zxx} = \mathbf{-zyz} = \mathbf{-zzy}, zxy = zyx$ $\mathbf{xxx} = \mathbf{-yzy}, \mathbf{xyy} = \mathbf{yxx}, \mathbf{xzz} = \mathbf{-yzz},$ $\mathbf{xyz} = \mathbf{xzy} = \mathbf{yxx} = \mathbf{yzx}, \mathbf{xxz} = \mathbf{xzx} = \mathbf{yyz} = \mathbf{yzy},$ $\mathbf{txy} = \mathbf{-yyx} = \mathbf{xyx} = \mathbf{-yxy}, zxx = zyy, zzz,$ $\mathbf{zxx} = \mathbf{zxx} = \mathbf{zyz} = \mathbf{zzy}, \mathbf{zxy} = \mathbf{zyx}$
d	4	$1, 2_z, \pm 4_z$	$\bar{2}_x, \bar{2}_y, \bar{2}_{xy}, \bar{2}_{-xy}$	$\mathbf{xyz} = \mathbf{xzy} = \mathbf{-yxz} = \mathbf{-yzx},$ $xzx = xxz = yzy = yyz, zxx = zyy, zzz$
e	mm2	$1, 2_z, \bar{2}_x, \bar{2}_y$	$\pm 4_z, \bar{2}_{xy}, \bar{2}_{-xy}$	$xxz = xzx, yyz = yzy, zxx, zyy, zzz$
f	2	$1, 2_z$	$\bar{2}_x, \bar{2}_y$ $\pm 4_z, \bar{2}_{xy}, \bar{2}_{-xy}$	$\mathbf{xyz} = \mathbf{xzy}, \mathbf{xxz} = \mathbf{xzx}, \mathbf{yyz} = \mathbf{yzy}, \mathbf{yxx} = \mathbf{yxx},$ $zxx, zyy, zzz, \mathbf{zxy} = \mathbf{zyx}$ $xyz = xzy, xxz = xzx, yyz = yzy, yzx = yxz,$ $zxx, zyy, zzz, \mathbf{zxy} = \mathbf{zyx}$
g	mm2	$1, 2_z, \bar{2}_{xy}, \bar{2}_{-xy}$	$\pm 4_z, \bar{2}_x, \bar{2}_y$	$xxz = xzx = yyz = yzy, \mathbf{zxy} = \mathbf{xyx} = \mathbf{yzx} = \mathbf{yxz},$ $zxx = zyy, zzz, \mathbf{zxy} = \mathbf{zyx}$
h	m	$1, \bar{2}_y$	$2_z, \bar{2}_x$ $4_z, \bar{2}_{xy}$	$\mathbf{xxx}, \mathbf{xyy}, \mathbf{xzz}, \mathbf{xxz} = \mathbf{xzx}, \mathbf{yyz} = \mathbf{yzy},$ $\mathbf{yyx} = \mathbf{yxy}, zxx, zzz, \mathbf{zxx} = \mathbf{zxx}$ $\mathbf{xxx}, \mathbf{xyy}, \mathbf{xzz}, \mathbf{xxz} = \mathbf{xzx}, \mathbf{yyz} = \mathbf{yzy},$ $\mathbf{yyx} = \mathbf{yxy}, zxx, zzz, \mathbf{zxx} = \mathbf{zxx}$
i	1	1	2_z $\bar{2}_x$	All the elements are allowed: $\mathbf{xxx}, \mathbf{xyy}, \mathbf{xzz}, \mathbf{xyz} = \mathbf{xzy}, \mathbf{xxz} = \mathbf{xxz},$ $\mathbf{xxy} = \mathbf{xyx}, \mathbf{yxx}, \mathbf{yyy}, \mathbf{yzz}, \mathbf{yyz} = \mathbf{yzy},$ $\mathbf{yzx} = \mathbf{yxz}, \mathbf{yxy} = \mathbf{yyx}, zxx, zyy, zzz,$ $\mathbf{zyz} = \mathbf{zzy}, \mathbf{zxx} = \mathbf{zxx}, zxy = zyx$ $\mathbf{xxx}, \mathbf{xyy}, \mathbf{xzz}, \mathbf{xyz} = \mathbf{xzy}, \mathbf{xxz} = \mathbf{xxz},$ $\mathbf{xxy} = \mathbf{xyx}, \mathbf{yxx}, \mathbf{yyy}, \mathbf{yzz}, \mathbf{yyz} = \mathbf{yzy},$ $\mathbf{yxx} = \mathbf{yxx}, \mathbf{yxy} = \mathbf{yyx}, zxx, zyy, zzz,$ $\mathbf{zyz} = \mathbf{zzy}, \mathbf{zxx} = \mathbf{zxx}, \mathbf{zxy} = \mathbf{zyx}$
j	m	$1, \bar{2}_{-xy}$	$\pm 4_z, \bar{2}_{xy}, \bar{2}_{-xy}$ $2_z, \bar{2}_{xy}$ $4_z, \bar{2}_y$	no information about the parity $\mathbf{xxx} = \mathbf{yyy}, \mathbf{xyy} = \mathbf{yxx}, \mathbf{xzz} = \mathbf{yzz},$ $xyz = yxz = xzy = yzx, \mathbf{xxz} = \mathbf{xzx} = \mathbf{yyz} = \mathbf{yzy},$ $\mathbf{xxy} = \mathbf{yyx} = \mathbf{xyx} = \mathbf{yxy}, zxx = zyy, zzz,$ $\mathbf{zxx} = \mathbf{zxx} = \mathbf{zyz} = \mathbf{zzy}, zxy = zyx$ $\mathbf{xxx} = \mathbf{yyy}, \mathbf{xyy} = \mathbf{yxx}, \mathbf{xzz} = \mathbf{yzz},$ $\mathbf{xyz} = \mathbf{yxz} = \mathbf{xzy} = \mathbf{yzx}, \mathbf{xxz} = \mathbf{xzx} = \mathbf{yyz} = \mathbf{yzy},$ $\mathbf{txy} = \mathbf{xyx} = \mathbf{yyx} = \mathbf{yxy}, zxx = zyy, zzz,$ $zxx = zxx = \mathbf{zyz} = \mathbf{zzy}, \mathbf{zxy} = \mathbf{zyx}$
k	mm2	$1, 2_z, \bar{2}_x, \bar{2}_y$	-	$xxz = xzx, yyz = yzy, zxx, zyy, zzz$
l	m	$1, \bar{2}_x$	$2_z, \bar{2}_y$	$xzx = xxz, \mathbf{xyy} = \mathbf{xyx}, \mathbf{yxx}, \mathbf{yyy}, \mathbf{yzz},$ $yyz = yzy, zxx, zyy, zzz, \mathbf{zyz} = \mathbf{zzy}$
m	1	1	2_z $\bar{2}_x$	All the elements are allowed: $\mathbf{xxx}, \mathbf{xyy}, \mathbf{xzz}, \mathbf{xyz} = \mathbf{xzy}, \mathbf{xxz} = \mathbf{xxz}, \mathbf{xxy} = \mathbf{xyx},$ $\mathbf{yxx}, \mathbf{yyy}, \mathbf{yzz}, \mathbf{yyz} = \mathbf{yzy}, \mathbf{yzx} = \mathbf{yxz}, \mathbf{yxy} = \mathbf{yyx},$ $zxx, zyy, zzz, \mathbf{zyz} = \mathbf{zzy}, \mathbf{zxx} = \mathbf{zxx}, zxy = zyx$ $\mathbf{xxx}, \mathbf{xyy}, \mathbf{xzz}, \mathbf{xyz} = \mathbf{xzy}, \mathbf{xxz} = \mathbf{xxz}, \mathbf{xxy} = \mathbf{xyx},$ $\mathbf{yxx}, \mathbf{yyy}, \mathbf{yzz}, \mathbf{yyz} = \mathbf{yzy}, \mathbf{yxx} = \mathbf{yxx}, \mathbf{yxy} = \mathbf{yyx},$ $zxx, zyy, zzz, \mathbf{zyz} = \mathbf{zzy}, \mathbf{zxx} = \mathbf{zxx}, \mathbf{zxy} = \mathbf{zyx}$
n	2	$1, 2_z$	$\bar{2}_x, \bar{2}_y$	$\mathbf{xyz} = \mathbf{xzy}, \mathbf{xxz} = \mathbf{xzx}, \mathbf{yyz} = \mathbf{yzy}, \mathbf{yxx} = \mathbf{yxx},$ $zxx, zyy, zzz, \mathbf{zxy} = \mathbf{zyx}$
o	m	$1, \bar{2}_y$	$2_z, \bar{2}_x$	$\mathbf{xxx}, \mathbf{xyy}, \mathbf{xzz}, \mathbf{xxz} = \mathbf{xzx}, \mathbf{yyz} = \mathbf{yzy},$ $\mathbf{yyx} = \mathbf{yxy}, zxx, zyy, zzz, \mathbf{zxx} = \mathbf{zxx}$

p	6mm	$1, 2_z, \pm 3_z, \pm 6_z, 6(\bar{2}_\perp)$	-	$xxz = xzx = yyz = yzy, zxx = zyy, zzz$
q	6	$1, 2_z, \pm 3_z, \pm 6_z$	$\bar{2}_x, \bar{2}_y$	$\mathbf{xyz} = \mathbf{xzy} = -\mathbf{yxz} = -\mathbf{yzx}, xxz = xzx = yyz = yzy,$ $zxx = zyy, zzz$
r	3m	$1, \pm 3_z, \bar{2}_y, \bar{2}_{S(xy)}, \bar{2}_{S(-xy)}$	-	$zxx = zyy, xxz = xzx = yyz = yzy, zzz,$ $xxx = -xyy = -yxy = -yyx$
s	1	1	$\bar{2}_y$	All the elements are allowed: $xxx, xyy, xzz, \mathbf{xyz} = \mathbf{xzy}, xzx = xxz, \mathbf{xyx} = \mathbf{yxx},$ $\mathbf{yxx}, \mathbf{yyy}, \mathbf{yzz}, yyz = yzy, \mathbf{yzx} = \mathbf{yxz}, yxy = yyx,$ $zxx, zyy, zzz, \mathbf{zyz} = \mathbf{zzy}, zzx = zxz, \mathbf{zxy} = \mathbf{zyx}$
t	m	$1, \bar{2}_y$	-	$xxx, xyy, xzz, xxz = xzx, yyz = yzy,$ $yyx = yxy, zxx, zyy, zzz, zzx = zxz$
u	3	$1, \pm 3_z$	$\bar{2}_y$	$xxx = -xyy = -yxy = -yyx, \mathbf{xyz} = \mathbf{xzy} = -\mathbf{yxz} = -\mathbf{yzx},$ $xzx = xxz = yyz = yzy, \mathbf{xxy} = \mathbf{xyx} = \mathbf{yxx} = -\mathbf{yyy},$ $zxx = zyy, zzz$
w	1	1	-	All the elements are allowed

TABLE II. SHG response for all spin configurations of the (001) surface of a fcc lattice [48]. For the detailed description of the response types see Tab. I. The configurations are depicted in Fig. 1.

configuration	key (response type)
para	a
ferro1	b
ferro2	c
ferro4	d
AF:	
a), b), e), o)	e
c), f)	f
i), k), m), p)	g
r)	a

TABLE III. SHG response for all spin configurations of the (001) surface of a fcc lattice, with the spin structure of the second layer taken into account. For the detailed description of the response types see Tab. I. For the confs. see Fig. 1.

configuration	key (response type)
para	a
ferro1	b
ferro2	c
ferro4	d
AF:	
ax), ox)	h
ay), oy), r)	e
bx), by), ex), ey)	b
c), fx), fy)	i
i)	j
k)	f
m), p)	c

TABLE IV. SHG response for all spin configurations of the (110) surface of a fcc lattice [48]. For the detailed description of the response types see Tab. I. The configurations are depicted in Fig. 4.

configuration	key (response type)
para	k
ferro1	l
ferro2	m
ferro3	n
ferro4	o
AF:	
a), b), c), g) - l)	k
d), e), f)	n

TABLE V. SHG response for all spin configurations of the (111) surface of a fcc lattice [48]. Only one monolayer is taken into account. For the detailed description of the response types see Tab. I. The configurations are depicted in Fig. 5

configuration	key (response type)
para	p
ferro1	l
ferro3	o
ferro5	q
AF:	
a), i), k)	k
c), f)	n

TABLE VI. SHG response for all spin configurations of the (111) surface of a fcc lattice [48]. More monolayers are taken into account. For the detailed description of the response types see Tab. I. The configurations are depicted in Fig. 5.

configuration	key (response type)
para	r
ferro1	s
ferro3	t
ferro5	u
AF:	
a), i), k)	t
c), f)	u

TABLE VII. SHG response for all spin configurations of the (001) surface of a fcc lattice, distorted to a rhombohedral structure. For the detailed description of the response types see Tab. I. For the surface structure see Fig. 6, for the spin configurations see Fig. 1.

configuration	key (response type)
para	k
ferro1	m
ferro2	o
ferro3	l
ferro4	n
AF:	
a), b) - h), o)	n
i) - n), p) - r)	k

TABLE VIII. SHG response for all spin configurations of the (111) surface of a fcc lattice, distorted to a rhombohedral structure. Only one monolayer is taken into account. For the detailed description of the response types see Tab. I. For the surface structure see Fig. 6, for the spin configurations see Fig. 5.

configuration	key (response type)
para	k
ferro1, ferro4	l
ferro2	m
ferro3	o
ferro5	n
AF:	
a), k)	k
b) - j), l), m)	n

TABLE IX. SHG response for all spin configurations of the (111) surface of a fcc lattice, distorted to a rhombohedral structure. More monolayers are taken into account. For the detailed description of the response types see Tab. I. For the surface structure see Fig. 6, for the spin configurations see Fig. 5.

configuration	key (response type)
para	t
ferro1, ferro2, ferro4, ferro5	s
ferro3	t
AF:	
a), i), k)	s
b) - h), j), l), m)	t

TABLE X. SHG response for all spin configurations of the (001) surface of a fcc lattice, with one atom distinguished. For the detailed description of the response types see Tab. I. For the surface arrangement see Fig. 7. For the confs. see Fig. 1.

configuration	key (response type)
para	a
ferro1	b
ferro2	c
ferro4	d
AF:	
a), o)	h
b), e)	b
c)	f
f)	i
i), m), p)	e
k)	j
r)	d

TABLE XI. SHG response for all spin configurations of the (110) surface of a fcc lattice, with one atom distinguished. For detailed description of response types see Tab. I. For the surface arrangement see Fig. 7. For the confs. see Fig. 4.

configuration	key (response type)
para	k
ferro1	l
ferro2	m
ferro3	n
ferro4	o
AF:	
a)	l
b), c), h), i), k), l)	k
d)	1m
e), f), g)	n
j)	o

TABLE XII. SHG response for all spin configurations of the (111) surface of a fcc lattice, with one atom distinguished. Only one monolayer taken into account. For the detailed description of the response types see Tab. I. For the surface arrangement see Fig. 7. For the confs. see Fig. 5.

configuration	key (response type)
para	p
ferro1	l
ferro3	o
ferro5	q
AF:	
a)	l
c), f)	m
i)	o
k)	n

TABLE XIII. SHG response for all spin configurations of the (111) surface of a fcc lattice, with one atom distinguished. More monolayers are taken into account. For the detailed description of the response types see Tab. I. For the surface arrangement see Fig. 7. For the confs. see Fig. 5.

configuration	key (response type)
para	3r
ferro1	s
ferro3	t
ferro5	u
AF:	
a), c), f), k)	s
i)	t

TABLE XIV. SHG response for all spin configurations of the (001) surface of a fcc lattice, with a distortion of oxygen sublattice. For the detailed description of the response types see Tab. I. For the surface arrangement see Fig. 8. For the confs. see Fig. 1.

configuration	key (response type)
para	a
ferro1	b
ferro2	c
ferro4	d
AF:	
a), o)	h
b), e)	b
c), f)	i
i), k)	c
m)	j
p)	e
r)	d

TABLE XV. SHG response for all spin configurations of the (110) surface of a fcc lattice, with oxygen sublattice distorted. For the detailed description of the response types see Tab. I. For the surface arrangement see Fig. 8. For the confs. see Fig. 4.

configuration	key (response type)
para	k
ferro1	l
ferro2	m
ferro3	n
ferro4	o
AF:	
a), b), g), h), k), l)	k
c)	o
d), e), i), j)	n
f)	m

TABLE XVI. SHG response for all spin configurations of the (111) surface of a fcc lattice, with oxygen sublattice distorted. For the detailed description of the response types see Tab. I. For the surface arrangement see Fig. 8. For the confs. see Fig. 5.

configuration	key (response type)
para	u
ferro1, ferro3	w
ferro5	u
AF:	
All confs.	w